Identification of a Tendon Control System for Flexible Space Structures

Yoshisada Murotsu,* Hiroshi Okubo,† and Kei Senda‡
University of Osaka Prefecture, Sakai, Osaka 591, Japan

An experimental tendon control system is identified to make an accurate mathematical model for designing a controller. The experimental tendon control system has been constructed for the vibration control of a flexible beam simulating large space structures (LSS). The system has many low-frequency modes of vibration, and a modal survey requires lengthy testing. A proposed scheme needs time histories of responses for a very short period. First, a mathematical model of the system is developed through a finite element method (FEM). Second, unknown characteristic parameters are estimated by using an output error method. The validity of the proposed scheme is demonstrated by good agreement between the transfer functions of the experimental system and an identified model. Finally, the accuracy of the identified model is also verified by the agreement between the computed and the experimental closed-loop responses.

Introduction

LARGE space structures (LSS) are expected to have dynamic characteristics of high flexibility and low inherent damping owing to their large dimensions and lightweight construction materials. Therefore, the concept of active control of LSS has received a great deal of attention recently. In order to design a controller to meet prescribed closed-loop performance characteristics, an accurate model of the structure must be identified. It is very difficult to estimate structural parameters accurately because LSS will be developed and/or built on-orbit, and the unknown parameters have to be estimated.

Recently, modal survey testing methods to estimate modal parameters of structures have been studied and they are popularly used. But these methods are not always suitable for identification of LSS, because many sensors and actuators are needed and lengthy tests have to be carried out to identify such systems. Consequently, a method is desired for identifying LSS by the use of short tests and limited number of sensor outputs.

Some schemes are proposed to identify the structural parameters by using responses of vibrating systems, e.g., those by Sun and Juang,[1] Lee,[2] Banks and Crowley,[3] Meirovitch and Norris,[4] and Banks and Rosen,[5] and are based on numerical simulation. Only a few works use actual data; for example, the flexible mode characteristics of the Galileo spacecraft[6] and the structural parameters of the solar array from the Space Shuttle[7] are estimated. The results are acquired by specific methods and cannot be compared with other testing methods. For this reason, it is very important to identify some systems in a laboratory simulating a LSS and to compare the results with those generated by other methods.

In this paper, an experimental tendon control system is identified. The tendon control system has been proposed by the authors[8-10] for the vibration control of a beam-like space structure (Fig. 1). In order to investigate the feasibility of the control method, an experimental tendon control system has been built as shown in Fig. 1. A mathematical model of the whole system is developed through a finite element method (FEM). Based on the mathematical model, the unknown parameters are estimated to minimize the squared errors between the outputs of the actual system and the model. Outputs of responses just for a few seconds measured by a few sensors are used. The validity of the mathematical model thus obtained is demonstrated by agreement between the transfer functions of the experimental system and an identified model. The accuracy of the identified model is also verified by the agreement between the computed and the experimental closed-loop responses.

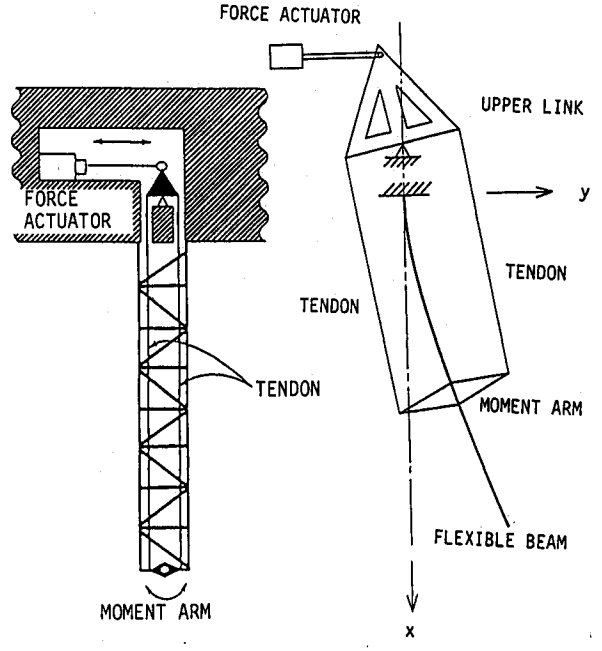

Fig. 1 Tendon control system for a beam-truss and the experimental system.

Presented as Paper 89-3568 at the AIAA Guidance, Navigation, and Control Conference, Boston, MA, Aug. 14-16, 1989; received Oct. 23, 1989; revision received March 1, 1990; accepted for publication May 28, 1990.

*Professor, Department of Aeronautical Engineering. Member AIAA.

†Lecturer, Department of Aeronautical Engineering. Member AIAA.

‡Research Associate, Department of Aeronautical Engineering. Member AIAA.

Experimental Apparatus

Figure 1 shows the tendon control system for the vibration of a highly flexible appendage structure deployed from a large spacecraft bus. The system consists of a torque generating part placed at the spacecraft main body, a pair of moment arms attached to the structure at a proper location, and tensile cables (tendon wires) for the linkages between the torquer and the moment arms.

Tendon experimental research has been conducted by using a laboratory structure and a prototype tendon control system (Fig. 1). The test structure used for the experiment is a clamped-free homogeneous stainless-steel beam hanging in the vertical direction. The beam has extremely high flexibility with the lowest five vibration modes under 10 Hz. Hardware devices for the control experiment are briefly described in the following. (For details see Refs. 8 and 9.)

Tendon Actuator System

As illustrated in Fig. 2, the prototype tendon control system consists of three parts: an electrodynamic actuator with a rotary upper link, a pair of moment arms mounted on the beam, and tensile cables (tendon wires) connecting the link to both ends of the moment arms.

The rotation link is utilized to convert the linear actuator force into torque and to operate a pair of tendons in a differential way. The moment arms are made from an aluminum plate and mounted on the test beam at the 60% point along the beam length from the root. The tension cables are made of piano wire of 0.35 mm diameter, with a rigidity of $k_t = 1.08 \times 10^4$ N/m. Each cable is subjected to an initial tensile force of an appropriate magnitude to prevent slack in the cables during the control action and to keep the total axial load applied to the beam nearly constant.

Measurement System

Electro-optical position-sensing devices (PSDs) and light-emitting-diode (LED) targets are used to measure the rotational motion of the upper link or the moment arms. Eddy-current type displacement transducers are also used for measuring the transverse displacement of the beam. Only the rotational measurement of the upper link is used for the control.

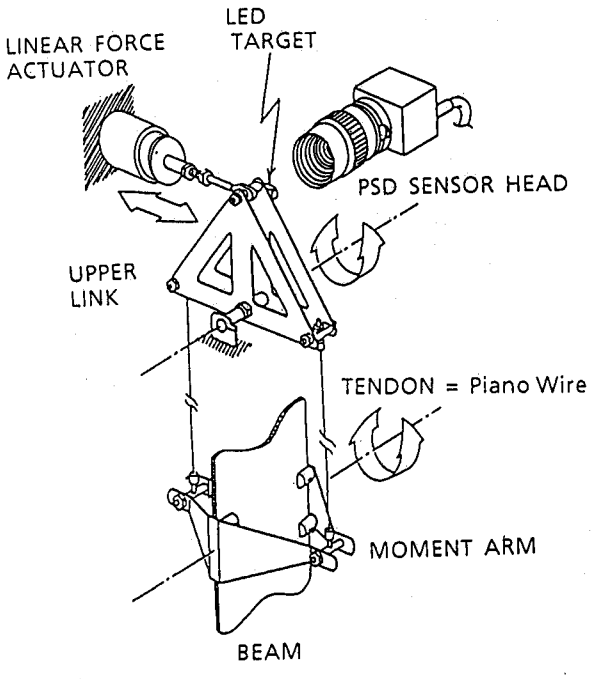

Fig. 2 Hardware setup for the tendon actuator.

Transfer Functions

Modal survey tests were carried out by using a fast Fourier transform (FFT) analyzer, and the obtained mechanical compliance or transfer functions, i. e., G_{LL} and G_{LM} are shown in Figs. 3a and 3b. G_{LL} and G_{LM} denote, respectively, the transfer function from the input torque M_L to the deflection angle of the upper link Θ_L and the input torque M_L to the angular deflection at the point of the moment arm Θ_M. Since the test structure has very low damping, the gain plots in Fig. 3 show many large peaks at the resonant frequencies over a wide range of frequencies. There are 17 resonant peaks under 100 Hz. As illustrated in Fig. 4, the dynamics of the tendon actuator become significant for mode numbers greater than 10. Furthermore, as illustrated in Fig. 3b, the phase of the experimentally derived transfer function G_{LM} moves into -180 to -360 deg region for mode numbers greater than the eleventh, which implies that the rotations of the upper link and moment arms are in near-opposing directions.

Modeling of the Dynamics

Equations of Motion

The equations of motion are derived for the coupled dynamics of the beam/tendon-actuator system. Parameters of the experimental setup are illustrated in Table 1 and Fig. 5. The equation for the transverse displacement of the beam $y(x,t)$ is

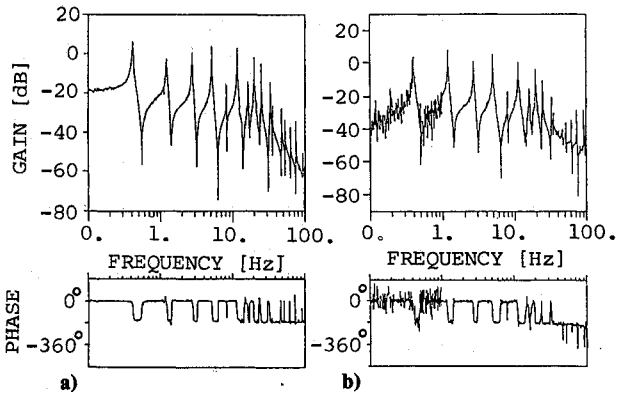

Fig. 3 Measured frequency-transfer functions: a) G_{LL}; and b) G_{LM}.

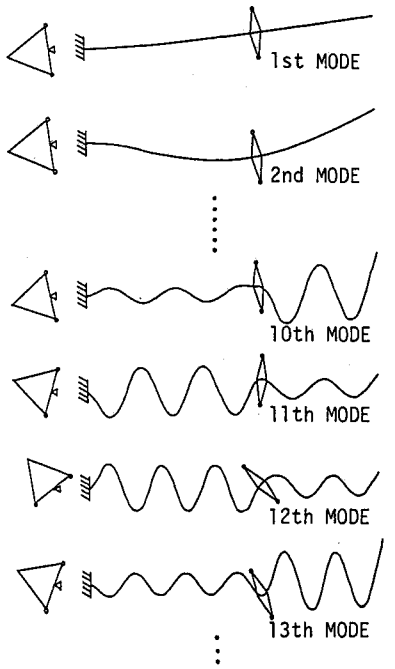

Fig. 4 Analytically predicted mode shapes for the tendon control system.

Table 1 Parameters of the experimental setup

$EI \doteq 2.4$, Nm^2		$\rho A = 1.156$, kg/m
$L = 2.4$, m	$L_M = 1.44$, m	$a = 0.26$, m
$r_a = 0.10$, m	$r_G = 0.065$, m	$k_t = 1.08 \times 10^4$, Nm
$m_L = 0.245$, kg		$I_L = 3.37 \times 10^{-3}$, kg/m^2
$m_M = 0.163$, kg		$I_M = 4.07 \times 10^{-4}$, kg/m^2

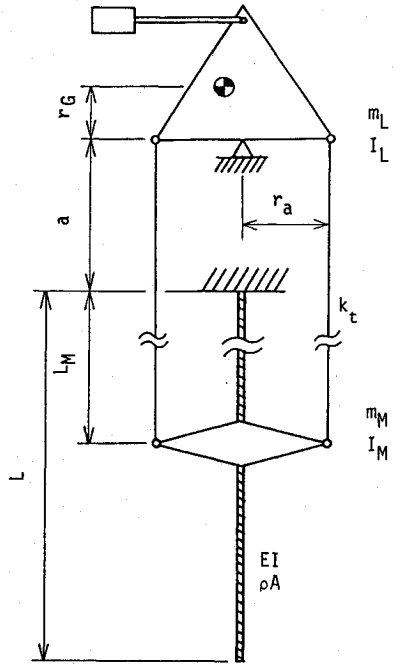

Fig. 5 Parameters of the experimental setup.

given by Euler-Bernoulli theory. Since the test beam is supported in the vertical direction, gravity has the effect of increasing the natural frequencies, especially the low-frequency modes. The static load due to the tensile force in the tendons is also taken into consideration. The partial differential equation governing the dynamics of the beam with the gravitational force $\rho Ag(L-x)$ and the static axial load $T(x)$ applied through the tendons is written in the form

$$\rho A \frac{\partial^2 y}{\partial t^2} + \rho A \alpha \frac{\partial y}{\partial t} + EI\beta \frac{\partial^3 y}{\partial t \partial x^2} + EI \frac{\partial^4 y}{\partial x^4} + T(x) \frac{\partial^2 y}{\partial x^2} - \frac{\partial}{\partial x}\left\{\rho Ag(L-x) \frac{\partial y}{\partial x}\right\} = F_c \tag{1}$$

where

$$F_c = -\frac{\partial M_c}{\partial x} \tag{2}$$

and

$$T(x) = T, \qquad 0 \le x \le L_M$$

$$T(x) = 0, \qquad L_M < x \le L$$

where ρA and EI are the mass density per length and flexural rigidity of the beam, respectively. In addition, F_c and M_c are the applied control force and torque, respectively. The control torque is applied to the beam through the moment arms, which is expressed as $M_c = M_M \delta(x - L_M)$, where δ is the Dirac delta function. The boundary conditions for $x = 0$, $x = L_M$, and $x = L$ are given by

$$y = \frac{\partial y}{\partial x} = 0, \qquad x = 0 \tag{3}$$

$$EI \frac{\partial^2 y}{\partial x^2} - M_M = 0, \qquad EI \frac{\partial 1^3 y}{\partial x^3} + T\left(\frac{\partial y}{\partial x} - \frac{y}{L_t}\right) = 0, \qquad x = L_M \tag{4}$$

$$EI \frac{\partial^2 y}{\partial x^2} = 0, \qquad EI \frac{\partial^3 y}{\partial x^3} = 0, \qquad x = L \tag{5}$$

where M_M and L_t are the torque applied by the tendon actuator and the length of the tendon wire ($L_t = L_M + a$ in Fig. 5), respectively.

Dynamics of Tendon Actuator

The dynamics of the rotary link and tension cables is modeled as a single degree-of-freedom vibrating system consisting of a rotating body with viscous damping and a linear spring. The equation of motion for the angle of the rotary link θ_L is written as

$$\ddot{\theta}_L + 2\zeta_L \Omega_L \dot{\theta}_L + \Omega_L^2 \left\{\theta_L - \left.\frac{\partial y}{\partial x}\right|_{x=L_M}\right\} = M_L \tag{6}$$

where

$$\Omega_L = \sqrt{2k_t r_a^2 / I_L} \tag{7}$$

$$2\zeta_L \Omega_L = d_L / I_L \tag{8}$$

with k_t, I_L, r_a, and d_L as the spring constant of the tendons, the moment of inertia of the link, the length of effective moment arm, and the viscous damping coefficient of various sorts, respectively. M_L denotes the control torque applied to the link. The torque applied to the moment arms M_M is given by

$$M_M = 2k_t r_a^2 \left\{\theta_L - \left.\frac{\partial y}{\partial x}\right|_{x=L_M}\right\} \tag{9}$$

Finite Element Method Model

A finite element method (FEM) is employed for discretizing the system and developing the ordinary differential equations expressing the dynamics. The stiffness matrix includes the contributions of the gravitational force and the static axial load. The ordinary differential equations for the beam and tendon actuator are written in a vector form (for details see Appendix A):

$$M\ddot{y} + D\dot{y} + Ky = f \tag{10}$$

where the $(2N+1)$-vector y consists of the elemental displacement and gradients for the beam $[y_i = y(x_i),\ y_i' = (\partial y/\partial x)_i,\ i = 1, \ldots, N]$ and the angle of link rotation θ_L. The matrices M, D, and K are the mass, damping, and stiffness matrices, respectively. The total mass matrix M and stiffness matrix K are functions of the parameters ρA and EI as $M(\rho A)$ and $K(\rho A, EI)$. The damping is assumed to be linear, and the damping matrix D is the function of M, K, α, β, and d_L:

$$D = D(M, K, \alpha, \beta, d_L) \tag{11}$$

Hence, the equation of motion for the whole system Eq. (10) can be prescribed by the following parameter vector γ:

$$\gamma = \{\rho A, EI, \alpha, \beta, d_L\}^T \tag{12}$$

Parameter Identification

The unknown characteristic parameter vector $\gamma(N_P \times 1)$ is estimated by using the following procedure. The tendon control system is described with the state and the output equations

$$\frac{d}{dt}\begin{Bmatrix} y \\ \dot{y} \end{Bmatrix} = \begin{bmatrix} 0 & I \\ -M^{-1}K & -M^{-1}K \end{bmatrix}\begin{Bmatrix} y \\ \dot{y} \end{Bmatrix} + \begin{bmatrix} I & 0 \\ 0 & M^{-1} \end{bmatrix}\begin{Bmatrix} 0 \\ f \end{Bmatrix} \tag{13}$$

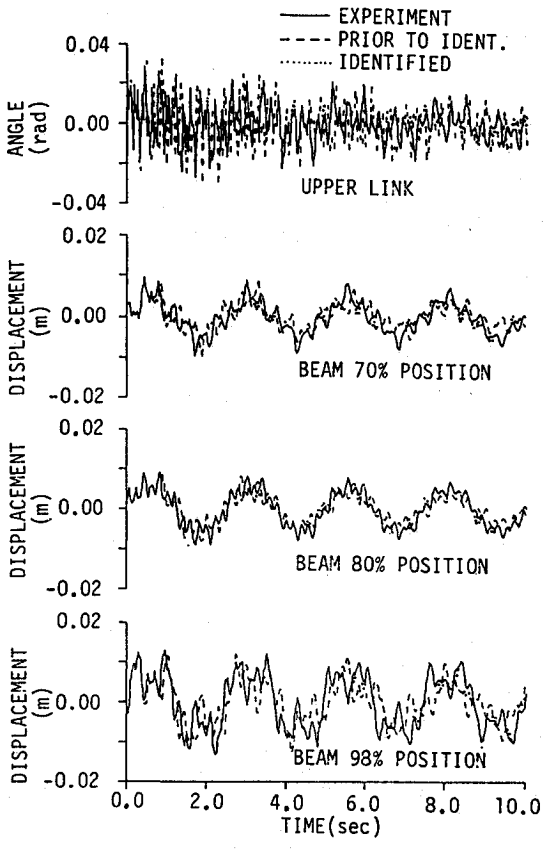

Fig. 6 Responses to the pseudoimpulse input.

$$z(t_k) = Cx(t_k), \qquad k = 1,2,\ldots,N_t \tag{14}$$

where $z(N_s \times 1)$ is an output vector that can be derived from the real system, and $x[(4N+2)\times 1]$ is a state vector $x = \{y^T \dot{y}^T\}^T$. Equation (13) is rewritten as

$$\dot{x} = Ax + Bu \tag{15}$$

The solution to Eq. (15) is given by

$$x(t_k) = \exp[At_k]x(0) + \int_0^{tk} \exp[A(t_k - \tau)]Bu(\tau)\, d\tau \tag{16}$$

If the input vector $u(t)$ is assumed to be a constant vector $u(t_{k-1})$ for Δt (from t_{k-1} to t_k), then $x(t_k)$ is given by

$$x(t_k) = \Psi x(t_k - 1) + \Pi u(t_{k-1}) \tag{17}$$

where

$$\Psi = \exp[A\,\Delta t] \tag{18}$$

$$\Pi = (\Psi - I_{4N+2})A^{-1}B \tag{19}$$

Since $x(0)$ is known, $x(t_1), x(t_2), \ldots$ are sequentially computed by using Eq. (17). In the numerical examples of the following section, Δt is set to 2 ms and Ψ is approximated by a Taylor series up to the 15th order. Accuracy of this method is verified by comparing the solution with those generated by other methods, e.g., the Runge-Kutta method.

The tendon control system is in static equilibrium at initial time, so that $x(0) = 0$, $z(0) = 0$. The tendon control system is excited by applying a known signal to the tendon force actuator and the output vector $z(t_k)$ is measured. The mathematical model, Eq. (13), is subject to the same excitation and its numerical solutions are obtained with the computer. An error vector is given by

$$\nu(t_k) = z_m(t_k) - z_a(t_k) \tag{20}$$

Table 2 Estimated parameters

	EI, Nm^2	ρA, kg/m	α, 1/s	$\beta \times 10^{-4}$, s	$d_L \times 10^{-4}$, Nsm
Predicted	1.930	1.156	0.1336	0.30	0
Undamped frequencies	2.417	1.156	—	—	—
Pseudoimpulse	2.462	1.156	0.0396	1.20	4.26
M-sequence 1	2.418	1.156	0.0387	0.95	2.82
M-sequence 2	2.460	1.156	0.0150	0.25	7.94

where $z_m(t_k)$ and $z_a(t_k)$ are the outputs of the mathematical model and the actual system, respectively. Then, the performance index is defined by

$$J = \sum_{k=1}^{N_t} \nu(t_k)^T W(t_k) \nu(t_k) \tag{21}$$

where $W(t_k)$ is the weighting matrix. In the numerical examples of the next section, the identity matrix $I_{Ns}(N_s \times N_s)$ is employed for $W(t_k)$, and ν is computed every 4 ms. The unknown parameter vector γ is determined such that the performance index is minimized by using a standard optimization method, e.g., Davidon-Fletcher-Powell method.[11] The optimization problem is solved under the constraints

$$\alpha \geq 0, \qquad \beta \geq 0, \qquad d_L \geq 0 \tag{22}$$

Experimental and Identified Results

In the experimental identification, the responses of the angle of the upper link and displacement measurements of the beam are sampled every 4 ms, and time histories of the responses for 6 s are used for the identification. The mathematical model used to identify the parameters is a 10-element FEM model for the flexible beam ($N = 10$). The mass density per length ρA has been measured, so that the parameter vector γ to be estimated is reduced to

$$\gamma = \{EI, \alpha, \beta, d_L\}^T \tag{23}$$

Input Signals

A pseudoimpulse and the M-sequence are used to excite the system. The pseudoimpulse is a rectangular pulse that has 0.525 Nm torque and 57.5 ms length. The M-sequence signal, proposed by Huffman,[12] is a pseudorandom binary signal that has the following characteristics: 1) It is a periodic signal that is generated by a simple method and also has the characteristics of white noise. 2) The power required to generate it is smaller compared with that of an impulse.

Results of Parameter Estimation

Case of Using Pseudoimpulse

The time histories of the pseudoimpulse response are shown in Fig. 6. The predicted responses previous to the identification are also shown in Fig. 6. The parameters designated as "Predicted" in Table 2 are determined as follows. EI is predicted from the material and dimensions of the beam based on the method of Ref. 13. The d_L is assumed to be zero, and α and β are determined so as to minimize the squared error between the damping ratios of the modeled and measured system. The responses of the identified model are in better agreement with the experimental results than the predicted responses. The identification improves the mathematical model. The estimated parameters are listed in Table 2, where ρA is fixed to be the measured value. The modal frequencies and damping ratios are listed in Table 3 together with the experimental values. The modal damping ratios are measured up to the 8th mode by using harmonic excitation tests and decays of free responses.

Case of Using M-Sequence

Two types of M-sequence input are used for the identification. The method to generate M-sequence signals used here is described in the Appendix B. The time histories of measured responses to M-sequence 1 input are illustrated in Fig. 7. The M-sequence signal is generated from time = 0. The responses from the predicted and identified models are also shown in Fig. 7, which shows that the identified responses agree well with the actual responses. The estimated parameters used for M-sequences 1 and 2 are given in Table 2. The estimated modal frequencies and damping ratios are listed in Table 3.

Evaluation of Identified Model

The value of *EI* designated as undamped frequencies in Table 2 is estimated in the following way: The system is assumed to have no damping and the parameter value is determined so as to minimize the squared error between the natural frequencies of the mathematical model and the measured ones up to the 9th natural frequency. This value is nearly equal to those estimated by the proposed methods. From the results listed in Table 2, it is observed that the estimated values of *EI* are almost the same in every case, while α, β, and d_L vary from case to case. Generally, damping parameters are estimated less accurately than those of the eigenfrequencies. Consequently, α, β, and d_L associated with damping are estimated less accurately than *EI* associated with the eigenfrequencies.

The pseudoimpulse is easy to generate but has the disadvantage that the signal excites the system only once at the initial period. In order to keep the power spectral density constant with proper magnitude up to high frequency, an impulse with large magnitude and short duration is required. But, it is generally impossible to generate such an impulse due to the limit of actuator power and/or structural weakness. In the present case, the limit of actuator power restricts the pseudoimpulse to be long. The M-sequence 2 keeps its power spectral density constant up to 200 Hz, but the powers of the pseudoimpulse and the M-sequence 1 decrease gradually over 10 Hz.

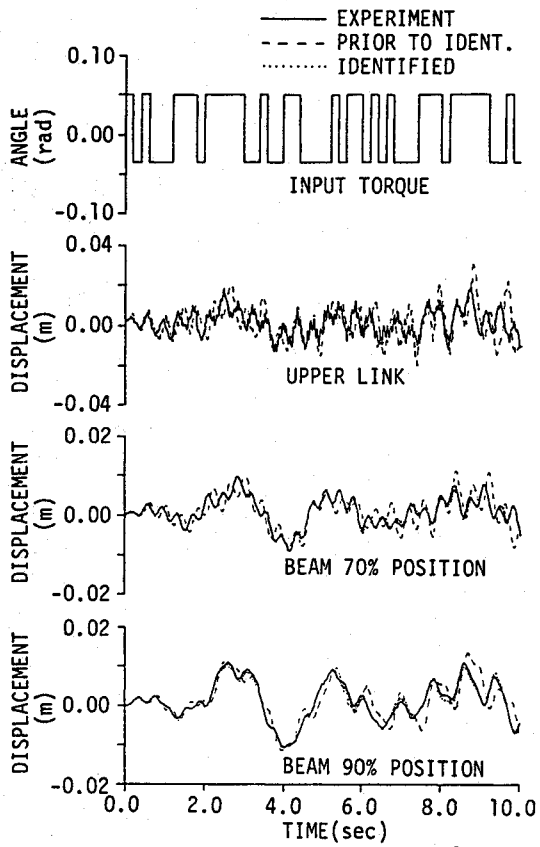

Fig. 7 Responses to the M-sequence input.

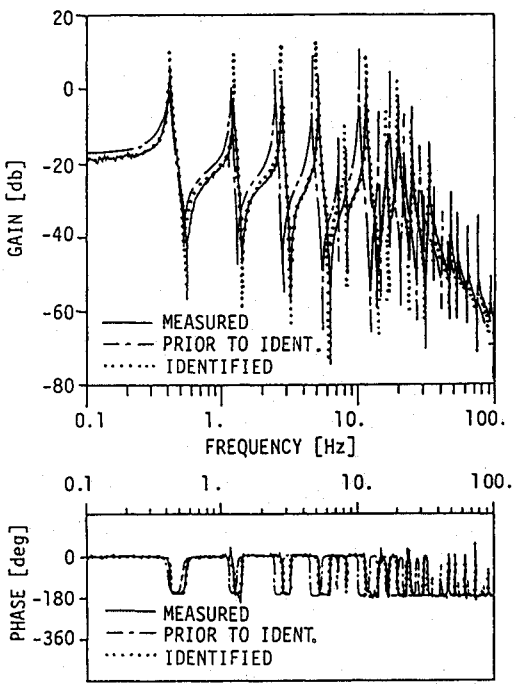

Fig. 8 Computed frequency-transfer function G_{LL} derived from the identified model.

Table 3 Modal frequencies and damping ratios

	Frequencies Ω_i, Hz				Damping ratios ζ_i			
		Identified				Identified		
Mode i	Measured	Impulse	M-sequence 1	M-sequence 2	Measured	Impulse	M-sequence 1	M-sequence 2
1st	0.407	0.407	0.404	0.405	0.011	0.0080	0.0078	0.0036
2nd	1.225	1.204	1.199	1.207	0.0041	0.0031	0.0029	0.0016
3rd	2.75	2.707	2.689	2.717	0.0040	0.0022	0.0020	0.0016
4th	5.10	5.054	5.015	5.061	0.0041	0.0026	0.0022	0.0022
5th	8.13	8.007	7.942	8.015	0.0016	0.0034	0.0028	0.0009
6th	11.50	11.42	11.33	11.43	0.0035	0.0047	0.0038	0.0042
7th	16.25	16.18	16.41	16.19	0.0017	0.0063	0.0050	0.0021
8th	20.0	19.50	19.35	19.51	0.0025	0.0076	0.0060	0.0047
9th	25.0	24.65	24.45	24.66	—	0.0094	0.0075	0.0031
10th	32.0	32.46	32.19	32.45	—	0.0123	0.0097	0.0033
11th	35.8	35.33	35.03	35.33	—	0.0134	0.0105	0.0029
12th	47.5	47.49	47.10	47.50	—	0.0179	0.0141	0.0039
13th	53.0	52.24	51.79	52.22	—	0.0197	0.0155	0.0041
14th	63.3	63.21	62.67	63.20	—	0.0238	0.0187	0.0050
15th	75.0	75.05	74.43	75.03	—	0.0282	0.0222	0.0059

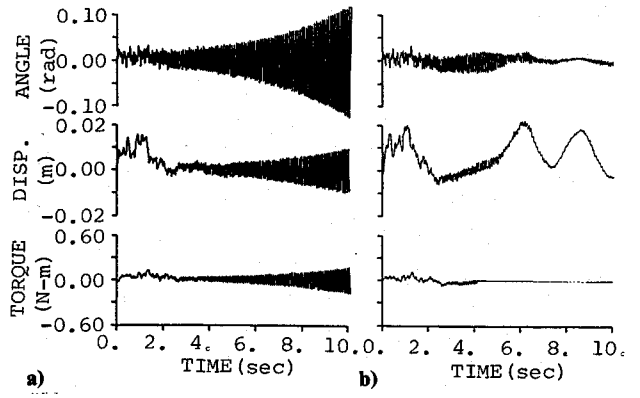

Fig. 9 Instability of a reduced-order controller: a) simulated; and b) experimental.

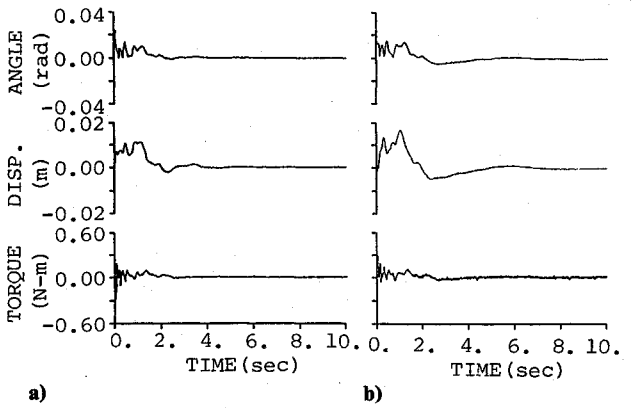

Fig. 10 Closed-loop responses of LAC/HAC: a) simulated; and b) experimental.

Consequently, the damping ratios of higher modes identified with the pseudoimpulse or the M-sequence 1 tend to be less accurate than those using M-sequence 2, as shown in Fig. 8 and Table 3.

The accuracy of the identified model is verified by comparing the frequency transfer functions and closed-loop responses of the identified model and the actual system. The model identified by using the pseudoimpulse is discussed in the following sections.

Evaluation by Transfer Function

The mechanical compliance G_{LL} computed with the predicted and identified models is illustrated in Fig. 8. The method to compute the transfer function G_{LL} is described in Appendix C. The measured transfer function is also illustrated in Fig. 8 for comparison. The agreement of the transfer functions between the identified model and the experimental results is satisfactory. It is also shown that the identification does improve the mathematical model since the identified transfer function is in better agreement with the measured one than the predicted one. But the damping ratios of the higher modes are estimated higher in comparison with the experimental results obtained from transient analysis. The most probable cause for this discrepancy is attributed to the characteristics of the output signal. Eddy-current type displacement transducers used here have 100 mm diameter, and the output is related to the average on that range. Consequently, wavy higher modes cannot be exactly observed by these sensors and their gains gradually decrease over the frequency of 20 Hz, as the higher modes are more difficult to excite.

Closed-Loop Response

Based on the identified model, a modern modal controller is designed and examined for the tendon control system using the collocated sensor/actuator at the upper link. A reduced-order modal controller that employs an eighth-order (4 modes) observer for the state feedback control is implemented. The feedback gains and the observer gains are designed through a pole-assignment approach so that the closed-loop poles of the regulator and those of the observer are placed at $-1\pm\Omega_i$ and $-2\pm\Omega_i$ ($i=1,2,3,4$), respectively, where Ω_i is the undamped natural frequency of the ith mode. The control law is realized by a control circuit with analog devices.

From the identified model, it is predicted that the closed-loop system would be unstable due to instability in the 6th and 8th modes (spillover instability). In fact, Figs. 9a and 9b show the computed and measured time responses of the closed-loop system after the pseudoimpulse is applied to the upper link through the control actuator, respectively. The control actuator was cutoff about 4 s after application of the impulse in order to avoid destructive motion. Hence, the 6th and 8th modes are identified accurately for designing the controller. In addition, Figs. 10a and 10b illustrate the computed and measured time responses of the stable closed-loop system for the low-authority control/high-authority control (LAC/HAC),[9] respectively. The impulsive disturbance applied through the control actuator is the same as in Figs. 9a and 9b. The direct velocity feedback (DVFB) gain for LAC is set as $K_v=0.4$ Nms for providing the system with increased modal damping especially in the 6th and 8th modes. Agreement between the computed and experimental results is satisfactory.

Conclusions

The experimental tendon control system has been identified. A mathematical model of the system has been developed using the finite element method. The tendon control system has been excited by a pseudoimpulse and M-sequence signals to the tendon force actuator, and its responses have been measured using a few sensors for a few seconds. Based on the mathematical model, the unknown parameters are identified so as to minimize the squared errors between the outputs of the actual system and the model. The transfer functions derived from the mathematical model are in good agreement with those obtained experimentally. The closed-loop responses for the controller based on the identified model have been simulated, and they are in good agreement with those from the experiments. The analytically and experimentally derived mathematical model approximates the real dynamics of the system with good accuracy.

Appendix A: Finite Element Method

First, the beam is divided equally into N finite elements with proper length L_i. The equation of motion of the ith element is given by

$$M_B\ddot{y}_i + D_B\dot{y}_i + K_B y_i = f_i \tag{A1}$$

where

$$y_i = \{y_{i-1}, y'_{i-1}, y_i, y'_i\}^T \tag{A2}$$

$$f_i = \{f_{i-1}, m_{i-1}, f_i, m_i\}^T \tag{A3}$$

M_B, D_B, and K_B are the element mass, damping, and stiffness matrices, respectively, and y_i, y'_i, f_i, and m_i are the transverse displacement, gradient, applied transverse force, and applied torque at the ith node, respectively. These matrices are derived using cubic interpolation functions as follows:

$$M_B = \frac{\rho A L_i}{420}\begin{bmatrix} 156 & 22L_i & 54 & -13L_i \\ & 4L_i^2 & 13L_i & -3L_i \\ & & 156 & -22L_i \\ \text{Symmetric} & & & 4L_i^2 \end{bmatrix} \tag{A4}$$

$$K_B = K_E + K_G + K_T \tag{A5}$$

$$D_B = \alpha M_B + \beta K_B \tag{A6}$$

where

$$K_E = \frac{2EI}{L_i^3}\begin{bmatrix} 6 & 3L_i & -6 & 3L_i \\ & 2L_i^2 & -3L_i & L_i^2 \\ & & 6 & -3L_i \\ \text{Symmetric} & & & 2L_i^2 \end{bmatrix} \tag{A7}$$

$$K_G = \frac{S_i}{30L_i}\begin{bmatrix} 36 & 3L_i & -36 & 3L_i \\ & 4L_i^2 & -3L_i & L_i^2 \\ & & 36 & -3L_i \\ \text{Symmetric} & & & 4L_i^2 \end{bmatrix} \tag{A8}$$

$$K_T = \frac{T_i}{30L_i}\begin{bmatrix} 36 & 18L_i & -36 & 3L_i \\ & 4L_i^2 & -3L_i & -L_i^2 \\ & & 36 & -18L_i \\ \text{Symmetric} & & & 4L_i \end{bmatrix} \tag{A9}$$

S_i and T_i are the gravitational load and the static axial load applied through the tendons, respectively. M_B and K_E are the mass and stiffness matrices of Euler-Bernoulli beam. K_G and K_T are the stiffness matrices that denote the contributions of the gravitational force and the static axial load applied through the tendons.

Second, the equation of whole beam is constructed from Eq. (A1), and the boundary conditions are considered. Based on Eq. (6), the elements of the tendon actuator are added, and the equation of motion of the whole system is given by

$$M\ddot{y} + D\dot{y} + Ky = f \tag{A10}$$

where

$$y = \{y_1, y_1', \cdots, y_N, y_N', \theta_L\}^T$$

$$f = \{f_1, m_1, \cdots, f_N, m_N, M_L\}^T$$

Appendix B: M-Sequence

A linear discretized system defined by the modulo two addition $\oplus$ and the normal product is given by

$$(z^{-n} \oplus a_1 z^{-n+1} \oplus \ldots \oplus a_{n-1} z^{-1} \oplus 1) u_t = y_t \tag{B1}$$

where u_t and y_t are defined on the linear space $\{0,1\}$, $a_i \in \{0,1\}$ $(i = 1,2,\ldots,n-1)$, and z^{-k} is defined as

$$z^{-k} u_t = u_{t-k} \tag{B2}$$

where k and t are round numbers. The system of Eq. (B1) is assumed to make a series of zero output: $y_t = 0$, and then Eq. (B1) is rewritten as

$$(z^{-n} \oplus a_1 z^{-n+1} \oplus \ldots \oplus a_{n-1} z^{-1}) u_t = u_t \tag{B3}$$

A series of u_t that satisfies Eq. (B3) is called null sequence and has a period of N. A null sequence that has the longest period to a given n is called M-sequence (maximum length null sequence), and has a period of $N_{\max} = 2^n - 1$.

The M-sequence 1 used in the numerical examples is generated from

$$(z^{-5} \oplus z^{-4} \oplus z^{-3} \oplus z^{-2}) u_t = u_t \tag{B4}$$

where the period is $N_{\max} = 31$, the initial values are 10110, and sampling time is 0.2 s. Based on this series of u_t, the generated signal shown in Fig. 7 is given by

$$X = \begin{cases} 0.415 \text{ Nm} & (u_t = 1) \\ -0.300 \text{ Nm} & (u_t = 0) \end{cases} \tag{B5}$$

Autocorrelation function of this signal is given by

$$\phi_{xx}(k) = \frac{1}{N} \sum_{t=1}^{N} X(t) X(t+k) \tag{B6}$$

$$= \begin{cases} 0.132 & (k = 0) \\ 0.0 & (k \neq 0) \end{cases} \tag{B7}$$

The M-sequence 1 is not well-designed, because the power spectral density has valleys every 5 Hz. Consequently, the 4th, 8th, and 9th modes are not easily excited.

The M-sequence 2 is generated from

$$(z^{-15} \oplus z^{-10} \oplus z^{-5} \oplus z^{-1}) u_t = u_t \tag{B8}$$

where the period is $N_{\max} = 232767$, the initial values are 1001101011110001, and sampling time is 4 ms. Based on this series of u_t, the M-sequence 2 is given by

$$X = \begin{cases} 0.0826 \text{ Nm} & (u_t = 1) \\ -0.0822 \text{ Nm} & (u_t = 0) \end{cases} \tag{B9}$$

This signal keeps the power spectral density constant up to 100 Hz.

Appendix C: Transfer Function

Using the derived mathematical model, the open-loop transfer function is derived. The equation of motion Eq. (10) is transformed into modal equation

$$y = \Phi q \tag{C1}$$

$$\ddot{q} + \Delta \dot{q} + \Lambda q = \Phi^T f(t) \tag{C2}$$

where

q = modal coordinate

$\Delta = \text{diag}[2\zeta_i \Omega_i] \quad (i = 1,2,\ldots,2N+1)$

$\Lambda = \text{diag}[\Omega_i^2] \quad (i = 1,2,\ldots,2N+1)$

Φ = M-normalized modal matrix

and Ω_i and ζ_i are the undamped natural frequency and the damping ratio of the ith mode, respectively. Laplace's transform of Eqs. (C1) and (C2) yields

$$Y(s) = \Phi(s^2 I + s\Delta + \Lambda)^{-1} \Phi^T F(s) \tag{C3}$$

Then, the mechanical compliance is obtained. For example, $G_{LM}(= \Theta_M / M_L)$ is given by

$$G_{LM}(\omega) = \sum_{i=1}^{2N+1} \phi_{Li} \phi_{Mi} / \{\Omega_i^2 - \omega^2 + 2\zeta_i \Omega_i (j\omega)\} \tag{C4}$$

where ϕ_{Li} and ϕ_{Mi} are the mode shapes of the ith mode associated with the upper link and the moment arm position, respectively.

Acknowledgments

This study is financially supported by a Grant-in-Aid for Scientific Research from the Ministry of Education, Science,

and Culture of Japan. The computations were performed using ACOS 850 at the Computer Center, University of Osaka Prefecture. The authors give their sincere thanks to A. Mitsuya, F. Terui, T. Yamaguchi, and Y. Araki for their help in the experimental work.

References

[1]Sun, C. T., and Juang, J.-N., "Parameter Estimation in Truss Beams Using Timoshenko Beam Model with Damping," *Proceedings of the Workshop on Applications of Large Space Structures,* Jet Propulsion Lab., Pasadena, CA, 1982, pp. 531–545.

[2]Lee, K. Y., "Techniques for the Identification of Distributed Systems Using the Finite Element Approximation," *Control and Dynamic Systems,* Vol. 27, Academic, San Diego, 1988, pp. 183–215.

[3]Banks, H. T., and Crowley, J. M., "Parameter Estimation in Timoshenko Beam Models," *Journal of Astronautical Sciences,* Vol. 31, No. 3, 1983, pp. 381–397.

[4]Meirovitch, L., and Norris, M. A., "Parameter Identification in Distributed Spacecraft Structures," *Journal of Astronautical Sciences,* Vol. 34, No. 4, 1986, pp. 341–353.

[5]Banks, H. T., and Rosen, I. G., "Computational Methods for the Identification of Spatially Varying Stiffness and Damping in Beams," *Control-Theory and Advanced Technology,* Vol. 3, No. 1, 1987, pp. 1–32.

[6]Wong, E. C., "In-Flight Identification of the Galileo Spacecraft Flexible Mode Characteristics," *Journal of Guidance, Control, and Dynamics,* Vol. 9, No. 1, 1986, pp. 92–98.

[7]Taylor, L. W., Jr., and Williams, J. L., "Distributed Parameter Modeling of the Structural Dynamics of the Solar Array Flight Experiment," *Proceedings of the AIAA Guidance, Navigation, and Control Conference,* Vol. 2, AIAA, New York, 1987, pp. 959–974.

[8]Murotsu, Y., Okubo, H., and Terui, F., "Low-Authority Control of Large Space Structures by Using a Tendon Control System," *Journal of Guidance, Control, and Dynamics,* Vol. 12, No. 2, 1989, pp. 264–272.

[9]Murotsu, Y., Okubo, H., Terui, F., Senda, K., and Shinoda, K., "Dynamics and Control of Experimental Tendon Control System for Flexible Space Structures," *Proceedings of the AIAA Guidance, Navigation, and Control Conference,* Pt. 2, AIAA, Washington, DC, 1988, pp. 852–860.

[10]Murotsu, Y., Okubo, H., Terui, F., Senda, K., and Shinoda, K., "Dynamics of Tendon Vibration Control System for Flexible Beam," *Transactions of the Japan Society of Mechanical Engineers,* Vol. 54, No. 507, Nov. 1989, pp. 2681–2688.

[11]Himmelblau, D. M., *Applied Nonlinear Programming,* McGraw-Hill, New York, 1972, pp. 111–121.

[12]Huffman, D. A., "The Synthesis of Linear Sequential Coding Networks," *Information Theory,* Academic, San Diego, CA, 1956, pp. 77–95.

[13]Sheafer, B., "Free Vibration of a Gravity-Loaded Clamped-Free Beam," *Ingenieur-Archiv,* Vol. 55, No. 1, 1985, pp. 66–80.